Nanostructured silicon geometries for directly bonded hybrid III-V-silicon active devices

Chengxin Pang, Henri Benisty

Nanostructured silicon geometries for directly bonded hybrid III–V-silicon active devices

C. Pang, H. Benisty *

Laboratoire Charles Fabry, Institut d'Optique Graduate School, CNRS, Univ Paris Sud, 2 Avenue Augustin Fresnel, 91127, Palaiseau, France

We discuss geometries with nanostructured cladding for active InP/silicon structures made by hetero-epitaxial bonding, which means that InP is directly bonded to silicon from a silicon-on-insulator without any intermediate layer. Such a cladding features low-index confinement and adds thermal sinking channels to those practised on the InP side. The first approach is a one-dimensional effective medium viewpoint, easily showing why grooves parallel to the waveguide are better. Then, two dimensional nanostructures are examined and found to perform better, given etching constraints. A more sophisticated geometry balancing thermal and optical confinement merits is then introduced thanks to a flip-flop algorithm.

Keywords: Hybrid silicon laser; Thermal management; Confinement; Silicon-on-insulator; Effective material

1. Introduction

The use of a silicon-on-insulator (SOI) platform in photonics has enabled several advances. Notably, it has allowed to implement photonic integrated circuits with active elements (lasers, amplifiers) thanks to the hybrid assembly of III–V, such as InP-based stacks, onto SOI-based waveguiding structures, as pioneered in 2006 [1–3] with continuous further successes [4–7]. In most such integration schemes, however, thermal management demands are hard to satisfy. Among the reasons is the fact that the heat generated typically by current injected in a multi-quantum-well active stack, that does not evacuate very well through the InP side, also encounters a heat barrier on the SOI side due to the systematic use of a thin isolating layer such as silica or BCB (Benzo-cyclo-butene) polymer [8,9] added in order ensure a reproducible bonding between the SOI and the flipped InP wafer piece.

It seems nevertheless possible to perform direct bonding, either at low temperature with molecular surface preparation [10] or at high temperature by direct heteroepitaxial bonding at 550 °C through properly prepared surfaces, the resulting bonded MQW retaining the original photoluminescence spectrum in a recent report [11], indicating a safe milestone towards active devices.

Such a situation calls for a specific engineering of the resulting device: because of the absence of any separation between, on one hand, the MQW/InP vertical waveguide and, on the other hand, the silicon waveguide, say a shallow ridge waveguide, Fig. 1(a), the coupled mode picture does not apply well. Of

* Corresponding author. Tel.: +33 1 6453 3286; fax: +33 1 6453 3318.

E-mail address: Henri.Benisty@insitutoptique.fr (H. Benisty).

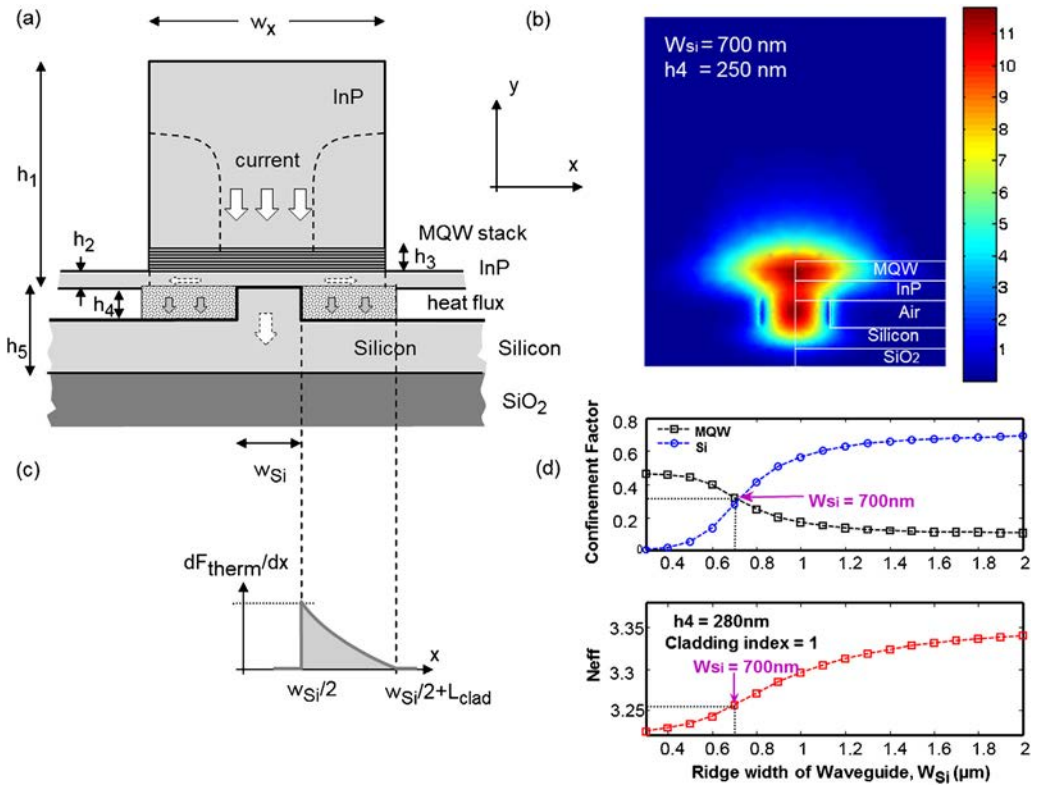

Fig. 1. (a) Cross-sectional view of the structure, with a vertical MQW/InP waveguide flipped on a ridge-type silicon waveguide, and parameters w_{Si}, w_x and h_1, h_2, h_3, h_4, h_5 as indicated; (b) calculated mode profile for air cladding on the ridge sides, h_5 is 500 nm, h_4 is 280 nm and w_{Si} is 700 nm. The structure is overlaid on the right side; (c) thermal weighting function aimed at favouring silicon close to the heat source; (d) confinement factors and effective index n_{eff} as a function of ridge width.

course, finding a guiding solution with a correct overlap of the gain layer and a good guidance by parametrically varying the ridge and MQW stack parameters is no serious difficulty, but as such, it would under-exploit the capability of the silicon on the SOI side: The cladding of the ridge can be made of nanostructured silicon (be it a shallow or a deep ridge) with an effective index just adequately low compared to the effective mode to be confined so as to preserve guidance, but with the clear interest of adding channels for heat sinking. As for the use of direct bonding to get current through to the silicon, it can also be envisioned in optoelectronics as well as in standard electronics, but an overall technology assessment against such options is beyond our scope.

The main scope of our contribution is to highlight which kind of extra cladding photonic nanostructures in this region adjacent to the core of the guiding structure may best serve the purpose of thermal sinking while not jeopardizing guidance itself: it is clear that at one extreme, with air aside the central ridge, confinement is good and thermal sinking is poor, while with homogeneous silicon, at the other extreme, thermal sinking is better but lateral confinement has just been lost. We will not go in any detail about the thermal models in our approach (we defer such details to further work) and will first deal with an effective medium approach [12,13]. Furthermore, we shall show here the validity of an adaptation of a quick and well-proven flip-flop optimization approach [14,15]. For our nanostructured cladding, we will assume that a vertical etch of constant depth has been practised such as grooves or cylindrical holes. We will thus use a simplified estimate thermal figure of merit F_{therm} of the structure, see Fig. 1(c). In its one-dimensional normalized version, easy to generalize to two-dimensional structures, we weigh the presence of thermal channels according to:

$$F_{\mathrm{therm}} = \frac{2}{L_{\mathrm{clad}}^2} \int_{w_{\mathrm{Si}/2}}^{w_{\mathrm{Si}/2}+L_{\mathrm{clad}}} P(x)\theta_{\mathrm{th}}(x)dx \qquad (1)$$

where $\theta_{\mathrm{th}}(x) = 1$ if there is silicon at point x, $\theta_{\mathrm{th}}(x) = 0$ otherwise, and $P(x)$ is a 3rd degree polynomial function pictured in Fig. 1(c) (restricted to the range indicated),

which is decreasing almost linearly, and whose details are unimportant insofar as we want to expose here the general aspects of our findings. In a later stage, we intend to build up this polynomial from the marginal thermal interest of a thermal bridge at position x.

On the photonic side, the confinement factors shall serve to build up the main photonic figure of merit and will be detailed below. Among the issues raised by these devices is the role of the polarization and the possible interest of the effective anisotropy of nanostructured silicon, i.e., the representation of this extra cladding as an effective material [12,13]. In the present work, we shall assume that we have the classical quasi-TE polarized gain in the MQW stack under adequate strains. For this reason, we shall essentially focus on the first TE-like fundamental mode. Given the interplay of lateral and vertical confinement in structures such as Fig. 1(a), the fundamental mode might in principle be y-polarized (i.e., quasi-TM) for a deep and thin ridge, in the limit $w_{\mathrm{Si}} \ll h_4 \approx h_5$. However, we will not examine such a limit. We have also made some investigation of higher-order mode solutions and will give a few details on that issue.

The paper is organized as follows: Section 2 gives a general discussion of the properties of nanostructured media for such thermally profitable cladding, starting with 1D nanostructuring (grooves) and considering next two-dimensional (2D) nanostructuring (photonic crystals). In Section 3, we consider a more refined optimization, whereby we perform optimization by a variant of the flip-flop technique well known in the area of filter design [14,15] for a texture consisting of etching more arbitrarily wide grooves.

2. Cladding with constant effective media

2.1. Basic structure description

Following the examples of Ref. [16] for hybrid amplifiers, we consider a rather thick SOI silicon layer, $h_5 = 500$ nm (Fig. 1(a)). For such a thick layer, a monomode operation is best obtained with a rather shallow ridge structure, with typical etch depth ranging from $h_4 = 300$ nm to $h_4 = 100$ nm. On the InP side, the MQW stack of equivalent optical index $n = 3.52$ is assumed to be relatively thick as well, $h_3 = 200$ nm, as needed for semiconductor optical amplifiers (SOA). The thickness of the thin InP layer covering the MQW (before being flipped) is assumed to be $h_2 = 200$ nm as well. The InP is taken of constant index $n = 3.17$. The height and width of the thick III–V part lying on top (after being flipped) are not important (they are around 2 μm or less in practice) as the mode is localized in the middle of it. More precisely, it can play a role for some secondary higher order modes. The main parameters for the situation without extra cladding are thus the ridge height h_4 and the ridge width w_{Si}. The silicon index is taken to be dispersionless at $n_{\mathrm{Si}} = 3.5$, as the results are not much influenced by this aspect at our stage.

We thus vary the silicon width w_{Si} from 0.3 μm to 2 μm. The corresponding effective index and the variations of confinement factors in either the active region MQW (Γ_{MQW}) or the silicon waveguide (Γ_{Si}) are shown in Fig. 1(d) for this structure that we call structure S1. We recall that the confinement factor is the fractional integral of the squared electric field of a guided mode. A typical working point of interest as a starting design at $\lambda = 1550$ nm is then the crossing point of the two confinement factors: it occurs at a width of $w_{\mathrm{Si}} = 700$ nm and gives balanced confinement factors $\Gamma_{\mathrm{MQW}} = \Gamma_{\mathrm{Si}}$ of around 0.32 and an effective index $n_{\mathrm{eff}} = 3.255$. It is for instance from such a starting point that tapers moving the guided wave to silicon or to InP are more easily designed.

In Fig. 1(b) is shown the typical $|E_x|^2$ field profile for this a structure S1 at this crossover. It will be a starting point in Section 2.2 for analysis of one-dimensional effective medium. The in-plane guidance is strong, made by air. The lateral field discontinuity in the shallow ridge part, normal to the sidewall, causes the bouncing of the profile in the air. This lateral guidance is indeed stronger than the vertical guidance, made by the silica bottom and the top InP, and indeed very narrow and less shallow ridges can have lateral confinement stronger than the vertical one.

Note that the mode shown in Fig. 1(b) shows that our structure could not be described as the coupling of two waveguides, as it would be a too drastic approximation. This is also logical because of the very close indices of the silicon and MQW stack ($\Delta n = 0.02$).

We shall also consider two other structures: S2 with $h_4 = 380$ nm for two-dimensional patterning, in Section 2.4 justified by the larger in-plane feature size in this case, and, in Section 3, a structure S3 with $h_4 = 300$ nm, for a similar reason. Both S2 and S3 will be based on a ridge width $w_{\mathrm{Si}} = 700$ nm.

2.2. One-dimensional effective medium

We now consider that the cladding is made of silicon etched with narrow trenches, at a subwavelength periodicity, making it an anisotropic effective medium [12,13]. Two possibilities to implement this idea are present in Fig. 2: In Fig. 2(a), we have the perpendicular

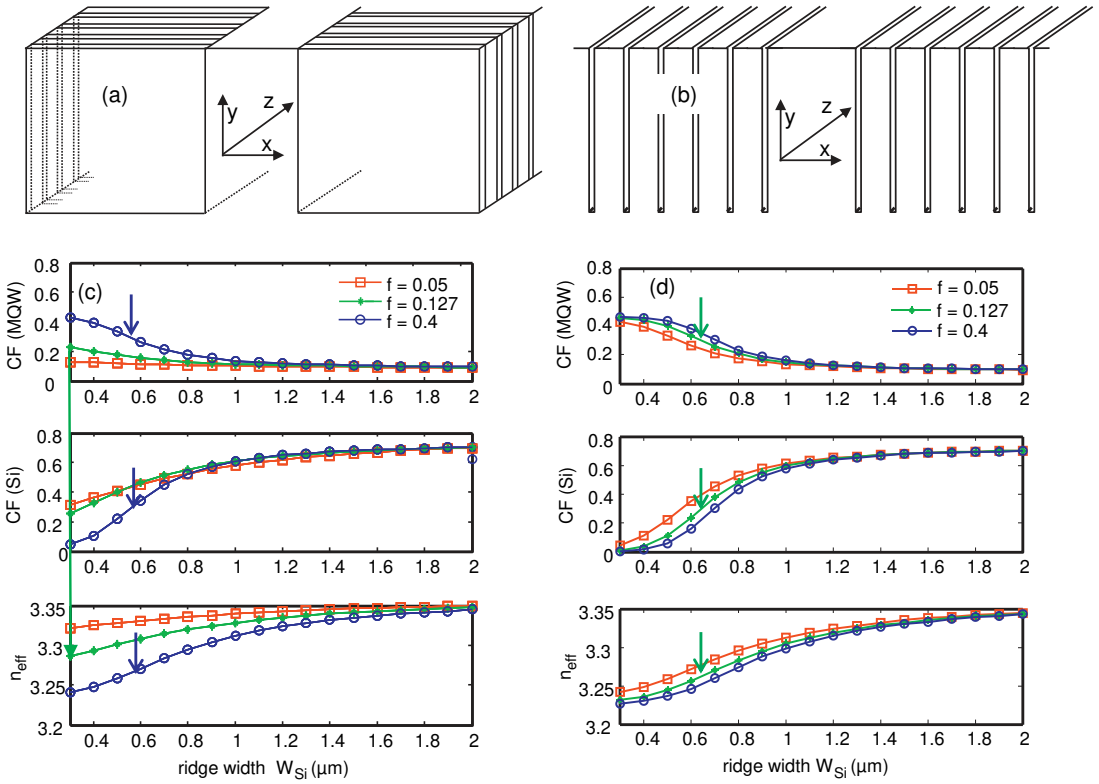

Fig. 2. One-dimensional nanostructured cladding; (a) perpendicular case A, with periodicity along the waveguide axis z; (b) parallel case B, with periodicity in lateral direction x and invariance along the guide direction z; (c) structure 1, case A, from top to bottom: confinement factors of Si, of MQW, and effective index n_{eff}, as a function of w_{Si} and for the three filling factors indicated. The arrows indicate the balanced Si/MQW confinement point for the case $f = 0.4$; (d) structure 1, now for B case. The arrows indicate the balanced confinement point for the case $f = 0.127$.

case A, with periodicity along the waveguide axis z. In Fig. 2(b), we have the parallel case B, with periodicity in lateral direction x and invariance along the guide direction z.

Let us first discuss realistic numbers for such structures: we operate around 1500 nm and effective indices of the order of $n_{\mathrm{eff}} = 3.25$ for the guided modes of interest. Obviously, in case A, we make sure that we have an effective medium if the period is less than the DFB (distributed feedback) period, or equivalently, that we operate below the first Brillouin zone edge in a longitudinal dispersion diagram $\omega(k)$ of the guided mode. The DFB period is $\Lambda = \lambda/2n_{\mathrm{eff}} \sim 231$ nm. We shall therefore assume periods of typically less than 210–220 nm.

As for the trench width, a lot depends on the basic structure. So, focussing on structure S1 that features $h_4 = 280$ nm ridge height, we may set a practical limit to etch depth associated to an aspect ratio such as 10. Thus, to etch the whole depth of 280 nm, we are constrained to trenches of width $w_{\mathrm{trench}} = 28$ nm or more. Therefore, we cannot have a higher index effective medium than what a 220 nm sequence such as 28 nm air/192 nm silicon offers us, or in other words, what an air filling factor $f \geq 0.127$ can do.

This implies an upper bound for the medium index. Assuming the silicon index to be $n = 3.5$, we know that in configuration A, we have to do a weighted average of the dielectric constants, whereas in configuration B, we have average of their inverse [12,13]. We therefore find, with a TE field assumed to be predominantly oriented along x, two different indices. Specifically, as shown in Table 1, we find that the largest effective index for A configuration is $n^{\mathrm{A}}_{\mathrm{em,max}} = 3.29$ $(= [f \times 1 + (1 - f)n^2_{\mathrm{Si}}]^{1/2})$, whereas for the B configuration, averaging ε^{-1}, we get the much lower index

Table 1
Effective index $n^{\mathrm{A}}_{\mathrm{eff}}$ (A configuration) and $n^{\mathrm{B}}_{\mathrm{eff}}$ (B configuration) vs. one-dimensional filling factors f.

Filling factor	0.050	0.127	0.400
$n^{\mathrm{A}}_{\mathrm{eff}}$	3.42	3.29	2.78
$n^{\mathrm{B}}_{\mathrm{eff}}$	2.80	2.24	1.49

value, $n^{B}_{em,max} = 2.24 (= [f \times 1 + (1 - f) n_{Si}^{-2}]^{-1/2})$. A logical consequence is that the compromise that we want to tackle between thermal sinking and confinement has a simple answer in that case: when silicon is added in the A configuration, we are at risk of delocalizing the mode because $n^{A}_{em,max}$ is so close from the targeted modal effective index with $f = 0.127$. We must then increase the air content, and diminish thermal conductivity. For instance, we have to go up to $f = 0.40$ (only 60% of silicon left) in this A configuration to get down to $n^{A}_{em,max} < 2.80$, a typical value that we found to limit well the role of higher order modes and to avoid diminishing the MQW confinement factor. Conversely, in the B configuration, sticking to this $n = 2.80$ index value as an upper limit, we calculate that there is a large yet formal margin down to $f = 0.05$ air fraction. There is therefore a large advantage to use B-type structures to enforce good confinement with high thermal sinking capability. In other words, even with the minimal air amount that can be practised to form our 1D nanostructured cladding, we are completely sure that the B structure shall result in fairly good confinement, whereas this is much more elusive in the A structure.

To make this more quantitative, and discuss the role of guide width with such nanostructured claddings, we illustrate in Fig. 2(c) the modal behaviour of the S1 structure, when we use for the cladding medium a uniform index of the A type (Fig. 2(a)). Namely, we plot the three key parameters for the A structure (Γ_{MQW} on top, Γ_{Si} below, and effective index n_{eff} at the bottom). We display similar data for a cladding medium made of a uniform index of the B type in Fig. 2(d). In both cases we allow ourselves to scan for three air-filling factors $f = 0.05$, $f = 0.127$, $f = 0.4$. The smaller value $f = 0.05$ might not be feasible with current etching technology for subwavelength grooves, but such a value will appear in a 2D context, thus the comparison will be instructive. Also, we have verified that there are indeed some differences between the present simulation of a uniform index and that of an actual anisotropic stack of Fig. 1(b) for the same targeted mode, but the main trends are much more quickly rendered by the present choice, with the added simplicity to avoid discussing the effect of the period.

If we look again at the point of intersection $\Gamma_{MQW} = \Gamma_{Si}$ to find a good working point, we see that in the A case, it can be done for $f = 0.127$ with $w_{Si} = 0.35$ μm or $f = 0.4$ with $w_{Si} = 0.6$ μm, but it is not feasible with $f = 0.05$ in the reasonable ridge width range. The trend towards narrower ridges can be explained by the fact that we now draw the overall field mode down thanks to the higher cladding index, so the relative occupancy of the silicon (Γ_{Si}) tends to increase at a given width, and this has to be compensated. The higher cladding index also means that the mode profile swells to a large degree, in other words, it is de-confined. This is the cause of the lower absolute value of both confinement factors, and could be considered as detrimental for many reasons. Therefore, quite some care should be exerted with this nanostructuring approach. To mitigate this de-confinement, it can be envisioned to shift to a larger ridge height, $h_4 > 280$ nm. The overall profile attraction of the silicon would then be moderated, and the confinement factors could be kept higher at lower air filling fraction, i.e., with better thermal sinking capabilities, and a higher thermal figure of merit F_{therm} (Eq. (1)). Another aspect is that, since the period to get the small f values would be close to the DFB period, we would be fully accurate only with a higher-order electromagnetic solution rather than an effective medium approach.

Indeed, we shall make use of such an accurate effective medium solution directly in the case of 2D nanostructures that we treat below. The reason to avoid spending more time on one-dimensional structures is their limits on the low f side, which are easily beaten by two-dimensional structures.

2.3. Two-dimensional effective medium

Here, we consider a two-dimensional nanostructure, essentially a photonic crystal in the subwavelength regime as shown in Fig. 3(a). For such a purpose, and to simplify the electromagnetic aspects, we prefer a square lattice photonic crystal. For tiny holes, etching limits are not as favourable as with trenches, and we shall assume that $d = 60$ nm is the smallest hole diameter for etch depths in the range $h_4 = 100$–380 nm. Then, for a period $a = 220$ nm, the air filling factor f can be as low as $f_{min} = \pi d^2/4a^2 = 0.058$. However, polarization and electromagnetic issues have to be taken into account. Using standard plane wave expansion for photonic crystal band structure calculations [17,18], we can obtain the effective (phase) indices $n^{2D}_{eff} = \omega/ck$ (usual notations) as a function of air filling factor f in a given crystallographic direction. We chose here ΓX, along the square lattice axis, in agreement with the predominant field direction in our geometry. To go to the largest possible period with a given feature (hole) size, it could seem advantageous to work with a wavevector along ΓM, at 45°, since the period between rows is apparently $\sqrt{2}$ smaller (the Brillouin zone limit at M, $\sqrt{2}\pi/a$, is $\sqrt{2}$ further from the Γ point than at X, $\Gamma X = \pi/a$). However, the important parameter regarding the

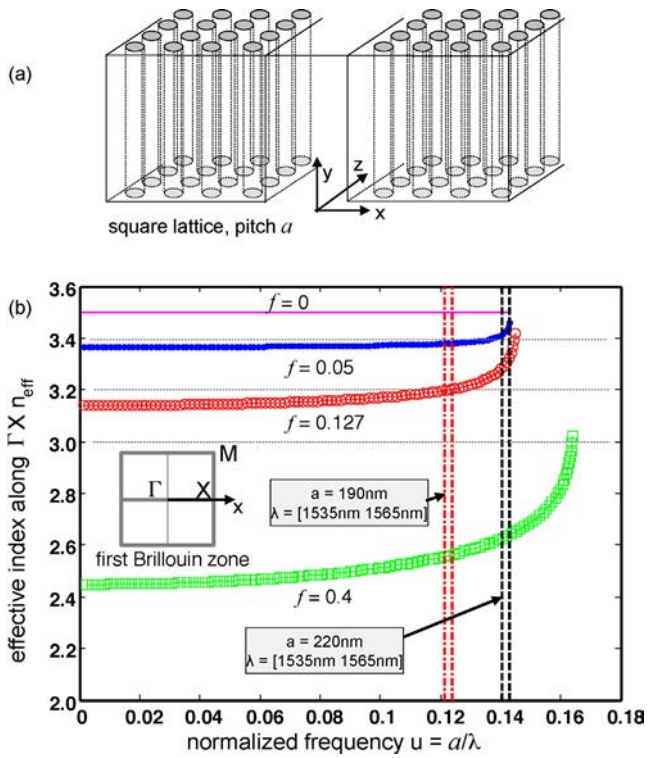

Fig. 3. Two-dimensional nanostructuring of the cladding; (a) scheme of the silicon ridge surrounded by a square lattice of holes of pitch a and of height h_4; the rest of the structure is omitted; (b) effective index of a 2D medium along the *X* direction of the first Brillouin zone, for four different air-filling factors, as a function of the normalized frequency. The correspondence with actual periods and the C-band of frequencies is indicated by the vertical line pairs.

presence or absence of DFB action is the index modulation period *along* the waveguide cutting in the middle of the photonic crystal, and not in a bulk photonic crystal. Such a ΓM configuration gives rise to a *longer* waveguide period $\sqrt{2}a$ along z, thus at risk of being in the DFB regime for our typical waveguiding effective indices of 3.25.

We plot in Fig. 3 the 2D effective cladding indices as a function of the normalized frequency $u = a/\lambda$, with the air-filling factor f as a parameter, for the four values indicated from $f = 0.00$ (''empty'' lattice, no holes) to $f = 0.40$. The long-wavelength limit is here $u \ll 0.1$, where the frequency does not affect the index. On the contrary, if we consider larger periods, we are in the range $u \sim 0.1$–0.15. Then the photonic crystal dispersion when approaching the band gap is sizable, and has to be taken into account. It could even be said that this nanostructured material's dispersion has to be taken into account in the telecom range for a typical C band transmission (say ∼1535–1565 nm), for instance in a limit case such as $u = 0.14$ and $f = 0.127$, where n_{eff} is close to 3.25–3.30 (see Fig. 3). It would still be a refinement of interest in the case $u = 0.14$ and $f = 0.4$. However we shall not take this dispersion into account. These issues should indeed have also been taken into account in the 1D case. However, for simplicity, we have focussed on the main information in the 1D case, namely the huge difference between the A and B structures, which essentially holds when the finite period of the subwavelength is considered.

Let us give a few hints on anisotropy, which we shall not take into account either: we note that at a frequency such as $u = 0.12$, the in-plane anisotropy of the band structure starts to be sizable ($\Delta n \sim 0.02$ between the two directions). It could impact the modelling, but again as a refinement. In addition, in our actual device geometry, there is also anisotropy not in the wafer plane xz, but considering off-plane fields, at an angle with the plane of periodicity. Such fields are sizable around the ''corners'' of the typical field profiles expected (Fig. 1(b)), but this can also be ignored compared to the other design issues at stake.

Exploiting now Fig. 3, we can interpolate from the set of curves that in the range $f = 0.1$–0.15, the effective index can easily be located in the range $n = 3.08$–3.25. The case $f = 0.127$ and $u = a/\lambda = 0.12$ with an effective

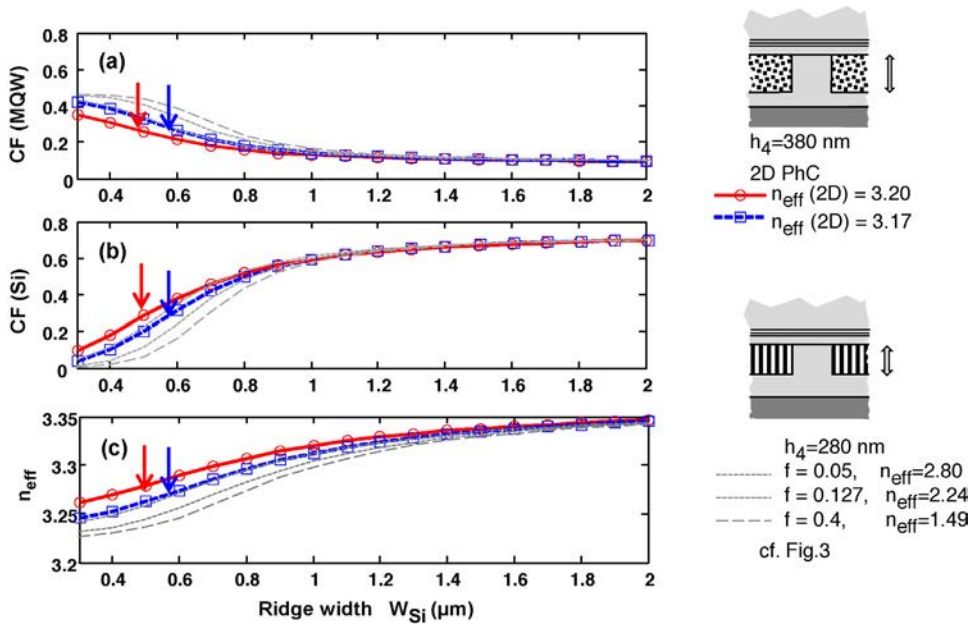

Fig. 4. Comparison of two-dimensional cladding and one-dimensional cladding. (a and b) confinement factors in the MQW and in the silicon as a function of ridge width; (c) effective indices. The 2D structures are depicted by the top right scheme and are assumed to have the 2D effective indices indicated, along a depth of 380 nm. Arrows indicate the balance point of equal confinement factors. The 1D structure and the corresponding plots in grey dashed lines are those of Fig. 2(b) and (d). The smallest f value of this set, $f = 0.05$, can hardly be distinguished from the curves of $n_{\text{eff}}(2D) = 3.17$. This shows that the small f regime (good for thermal behaviour) can be implemented with the larger feature sizes of the 2D nanostructuring with similar optical confinement.

index of less than 3.20 for instance corresponds to a period of 186 nm and a diameter $d = 75$ nm at $\lambda = 1550$ nm, making deep etching up to $h_4 \sim 400$ nm quite feasible ($h_4 < 6d$).

We can now revisit our global issue of improving the thermal conductivity through the cladding: if we go to smaller f for that purpose, our effective cladding index shall lay around 3.20, comparable to that of InP. Then, the mode profile, although it is feels attracted by the high index MQW stack on top, shall spread much more in the whole silicon bottom (ridge + cladding). We are then at risk of finding the same impediment as in the low-f one-dimensional A case with structure S1, namely too low confinement factors in the MQW.

So, we are led to consider ways to minimize the amount of silicon. Since the feature size of the holes (their diameter) is quite larger than those of grooves of equivalent f, etching somewhat deeper is feasible. We illustrate in Fig. 4 the success of such a design route, by choosing structure S2 with a depth $h_4 = 380$ nm, leaving only 120 nm nonpatterned silicon bottom. We first plot again the two confinement factors and the effective index of the structure as a function of silicon ridge width w_{Si}. We reproduce the results of Fig. 2(d) on the B case of the more shallow structure S1 as dashed grey lines with the textures indicated. It was seen in that case that the thermally interesting structures with the lowest f could be as low as $f = 0.05$. The cross-over of the silicon and MQW confinement factors indeed arose at around $w_{\text{Si}} = 560$ nm in that B case, and with an acceptable value of $\Gamma \sim 0.3$. But these structures were deemed to be not feasible because of the required groove width of $\sim$10 nm only for $\sim$200 nm period. Thus, in Fig. 4, running our mode solver for structure S2 ($h_4 = 380$ nm) and effective cladding indices of 3.17 and 3.20, we have plotted the resulting two sets of curves representing the same quantities as in Fig. 2(c) and (d). These two values are enough to illustrate the main trends. The case $n_{\text{eff}}^{\text{2D}} = 3.20$ corresponds to $f \approx 0.127$, $u = 0.124$, and thus to a period $a = 192$ nm at 1550 nm operation, and to a hole diameter $d = 77$ nm. The lower index case $n_{\text{eff}}^{\text{2D}} = 3.17$ corresponds to $f \approx 0.136$ for the same normalized frequency $u = 0.136$, and thus, for $a = 192$ nm, to a hole diameter $d = 80$ nm. We see that this latter case (square symbols) overlaps almost exactly with the previous $f = 0.05$ case, reminding that the difference is the depth, 380 nm instead of 280 nm. Therefore, by spreading the air in a two-dimensional fashion, even though we are loosing a part of the polarization properties that ensured a low cladding index for a small amount of air, we see

that we could restore feasible dimensions and achieve a good practical combination of high thermal conductivity and low enough index cladding. The key was to use the extra margin gained by the 2D patterning to etch deeper, thus maintaining the balance of the guided mode profile in silicon and in the MQW stack, as well as a decent absolute value of the confinement factor in the MQW itself.

Therefore, we have extended the feasible fabrication domain with the use of 2D nanostructured cladding: operating at 2D filling factors in the range $f = 0.1$–0.2 gives feature size in the 75–100 nm range that would correspond to about $f = 0.4$–0.5 with a one-dimensional arrangement. The price to pay is to etch a little deeper: This shall for a given in-plane pattern affect adversely the thermal sinking capability, but because the structure is truly two-dimensional, it shall also have a less anisotropic heat conduction than the series of grooves of structure B, which should eventually prove better because in these structures, heat sinking can clearly benefit from a substantial degree of lateral spreading.

In conclusion of our two studies on nanostructured cladding made from periodically etched silicon around the ridge, we see that A-type 1D structures with grooves normal to the waveguide, demand fairly high air filling factors and are thus detrimental for heat sinking. B-type 1D structures, with grooves parallel to the waveguide, could operate at lower filling factors, in the range $f < 0.15$, but, with a subwavelength period, this translates into too very narrow groove/slot widths, around 20–30 nm, say. But if we employ a square lattice of holes in the subwavelength regime again, we can easily implement low air filling factor and high thermal conductivity because of the 2D aspect, with much more feasible feature sizes in the 70–100 nm range. We loose a part of the benefit of the anisotropic 1D medium that was favourable to confinement in B structure of low air filling factor. But we can restore acceptable guiding conditions, notably confinement factor of the MQW high enough and balanced with that of Silicon, provided we etch somewhat deeper, around 380 nm in our example. This investigation of the main trends can be refined for actual devices with all their specific prescriptions. Its purpose was to lay out the main avenues for operating hybrid devices and taking advantage of the possibility of thermal sinking offered by the direct heteroepitaxial bonding between the InP-based chip and the silicon substrate.

To further exploit the full potential of nanostructuring, we can guess that an ideal approach would combine some of the benefits of the 1D and 2D approaches. Also, there is no specific reason to stick to a uniform effective structure in the normal (x) direction. We leave the first issue to further studies but we tackle the second point, leading to aperiodic nanostructures, in the last section.

3. Optimized "lamellar" cladding

Here, to investigate the potential of an aperiodic system, we start from the B-type 1D principle and show a route to optimize the cladding nanostructure with relatively arbitrary slot width and slot location.

Specifically, we use the 'flip-flop' algorithm [14,15] made popular in multilayer synthesis (so-called rugates), taking here into account the thermal management (figure of merit F_{therm}) and an optical figure of merit F_{phot}. For our targeted gain devices, it is important that in the competition with silicon for guidance, the field profile remains maximally in the MQW stack. However the absolute value of both confinement factors could vary in some limits, as the desired modal area eventually depend on the device investigated (SOA or laser, what level of losses is allowed, etc.). Therefore we will choose the ratio

$$F_{\mathrm{phot}} = \frac{\Gamma_{\mathrm{MQW}}}{\Gamma_{\mathrm{Si}} + \Gamma_{\mathrm{MQW}}} \tag{2}$$

as the figure of merit in the last section. The important point is to achieve a balance between a good optical behaviour and good heat sinking performance, privileging silicon regions that lie close to the guide core.

We briefly remind the flip-flop algorithm method, which proved effective to optimize antireflection coatings under spectral constraints [14,15]. One starts from a series of very thin layers with two indices, either low or high, and a merit function is defined towards the desired specification. Proceeding layer by layer, each layer is flipped from one material to the other, but the change is retained only if the overall figure of merit increases. After iterating such scans for a few loops, a structure with an acceptable local extrema of the figure of merit is obtained. A priori knowledge can often help to decrease the computational burden in the very first loops, but with the risk to miss unforeseen configurations.

We apply here the same method to vertical slabs of air or silicon constituting our cladding, i.e., in the encircled region indicated in Fig. 5(a). Thus, the refractive indices of silicon and air represent either higher index ($n_{\mathrm{Si}} = 3.5$) or low index ($n_{\mathrm{air}} = 1$). To evaluate the resulting structure, we calculate a total figure of merit F_{total}:

$$F_{\mathrm{total}} = F_{\mathrm{therm}} + bF_{\mathrm{phot}} \tag{3}$$

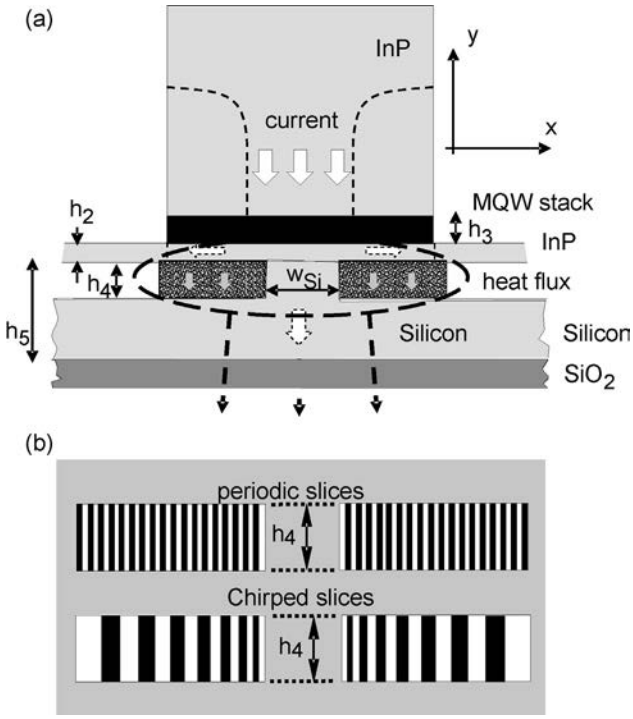

Fig. 5. (a) Same structure as Fig. 1, with the cladding region to be engineered encircled; (b) zoom of the two regions with two slice configurations for the flip-flop algorithm; top: periodic sequence configuration, bottom, chirped sequence configuration.

where b represents a weighting coefficient. In the present exercise whereby there is no full device model, we made the choice $b = 8$ because the thermal figure of merit varies over nearly unity among extreme configuration probed, whereas the optical figure of merit, for the cases of interest here, varies by only 0.1–0.15. We will use also this figure of merit to evaluate the composite 1D structures of variable filling factors discussed in Section 2. However, we start here from a structure that has a broad silicon ridge width w_{Si}, a case that is the less obvious to treat in the above approaches, see Fig. 4(a and b), since it appears to call for large air contents to restore a good optical figure of merit, thus likely to bring interesting design if treated otherwise. A full laser model or SOA model would of course exploit the amount of thermal sinking and the confinement factors to get for example the slope efficiency or the gain saturation, which are well known to depend on the above factors.

We have introduced a specific feature in our treatment, which can be viewed as originating from a priori knowledge in a broad sense: instead of a standard periodic set of elementary slabs (Fig. 5(b), top), we use a chirped sequence of slab thicknesses, see Fig. 5(b). Firstly, we know that the mode field is larger in the centre, thus making the choice of interface locations more critical. Thus, we prefer an accurate value for the first (broader) slot that plays a key role in confinement and thermal properties. So, slices below 10 nm can be advisable there. Secondly, we know that air slots smaller than a few tens of nm will be difficult to fabricate. We can take this typical size to dimension the thinnest actual slices, those that will consist of either thin air slots or thin silicon ridges. Along the same line, technology and waveguide practice suggests that we should avoid relying with a critical accuracy on slots widths at locations away from the structure's centre. This amounts to retain only structures with relatively wide slots/ridges that tend to bring a noncritical improvement in the external parts. For simplicity, we keep the central ridge width at 700 nm, and limit the overall width to 1840 nm. We also use these parameters to compare our optimized structures with those one-dimensional (1D) composite made according to type B geometry, in the spirit of an effective medium. A last reason to retain a relatively wide central ridge is to avoid locating the possibly rough sidewall interfaces at places in the field profile that still have a strong field. The last generic point is that we are now dealing with structure S3 as a basis, with the intermediate depth $h_4 = 300$ nm. Again, a (slightly) larger depth than in structure S1 is motivated by the hope to avoid the thinnest features.

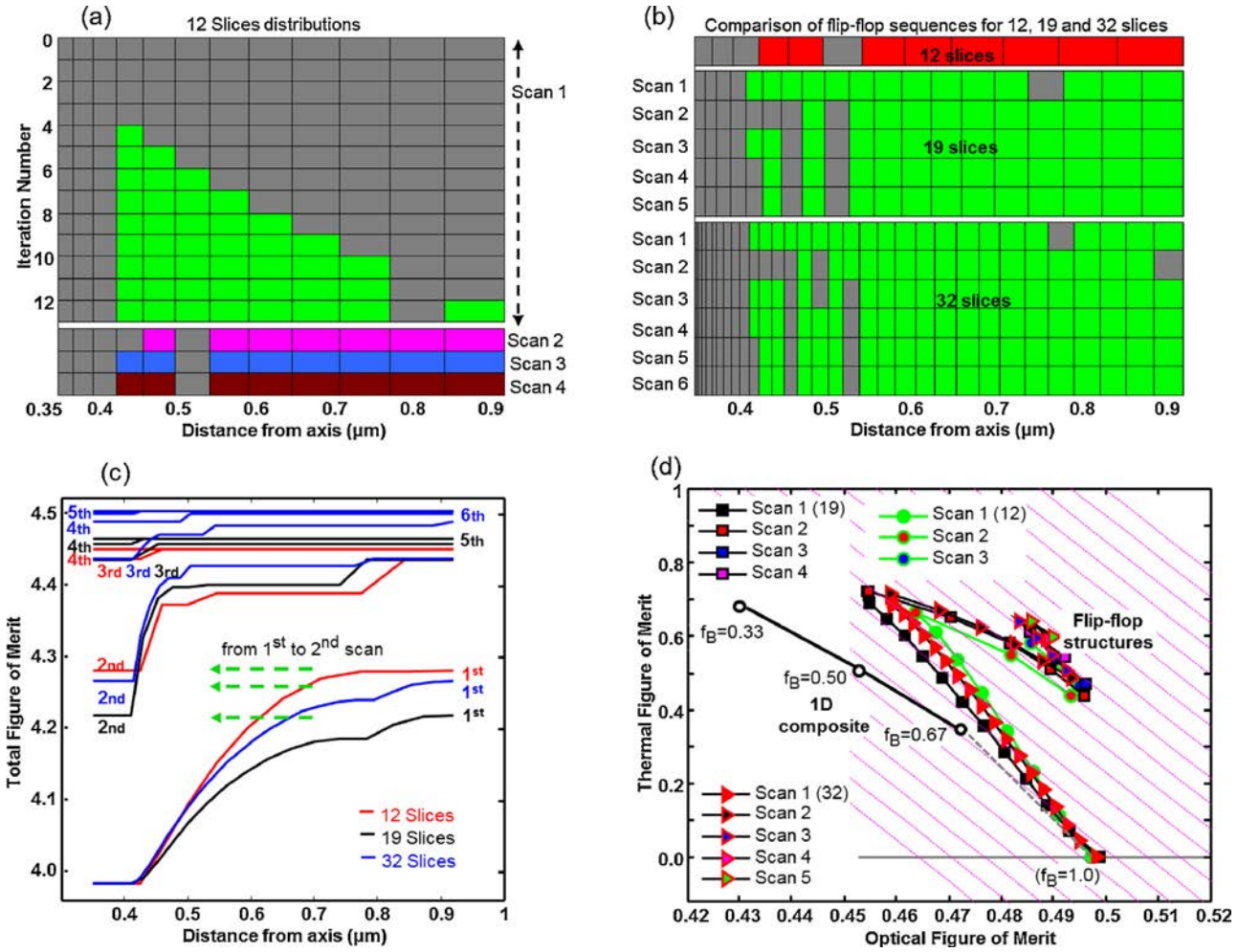

Fig. 6. (a) Distribution of Si/air during flip-flop scan sequence (grey: air, other colour: silicon) with detail of first scan (top rows) and results of scans 2–4 (bottom rows). (b) Comparison of Si/Air distributions for 12 [cf. panel (a)], 19 and 32 slices, with intermediate scan results. (c) Evolution of Figure of merit F_{total} as the flip-flop algorithm goes on, for the various number of slices. (d) Detailed evolution, of thermal and optical figure of merits. The oblique thin lines are for constant total figure of merit, growing to the top right, the various symbols are explained in the figure. The three empty discs connected by a solid line are the corresponding values for a 1D composite cladding of B type with air filling factors indicated, $f = 0.33$, 0.50 and 0.67, the case $f = 1$ corresponding to the full air cladding used also to start the flip-flop algorithm. (For interpretation of the references to colour in this figure legend, the reader is referred to the web version of the article.)

To test convergence, three examples with different initial widths and chirped values have been studied. The slice thicknesses of *example A* (12 slices) start from 20 nm and end at 75 nm with a 5 nm increment. Those of *example B* have 19 slices from 12 nm to 48 nm with 2 nm increment. The last case, *example C*, has 32 slices with a 1 nm increment only. In the top of Fig. 6(a) the first scan is unfolded pictorially: after the initial 75 nm of air (3 left slices), one can tile the subsequent slices with silicon, retaining a good confinement and improving thermal sinking. However, the penultimate slice eventually remains an air slot, as otherwise the amount of silicon would attract the mode too much towards silicon. In Fig. 6(c) the overall figure of merit F_{total} is seen to increase and saturate. At the subsequent scans, one obtains the distributions of the bottom of Fig. 6(a), whereby more air can be introduced closer to the silicon. The presence of silicon on the outer parts now dictates this route that could not emerge during the initial scan. Fig. 6(b) shows that F_{total} still increases notably during these modifications.

To get a quick idea of the potential and convergence of the method, we ran similar loops of scans for the examples B and C. The results of successive loops

appear in Fig. 6(b). We see that the trends are fully consistent with those manifested in case of 12 slices: an initial attempt to locate a thin air slot at the outside, followed by introduction of more air in the closer region. We now see that the flip-flop algorithm tries to build up an effective medium in the region from 0.4 to 0.6 μm, as physical intuition suggests: In the case of 19 slices, there are two air slots separated by a thin silicon ridge at abscissa $<\sim$0.5 μm. If we go to more slices (32 slices), the silicon ridges get thicker and the air slots remain one slice in width. This is in agreement with our initial 1D calculation suggesting that filling factors as low as 0.12 are effective. Here, we get a simpler design than by attempting to indeed force our flip-flop model towards a very high number of slices.

The details of the optimization are provided in Fig. 6(b) and (d). This latter plot shows best how the algorithm arbitrates between the two FOM. We can also see that the result is not much different between the two examples B and C, 19 and 32 slices. This also reinforces the relevance of our choice of relatively ''coarse graining'' models.

Finally, we added the simulation results of 1D composites of B-type to the plot of Fig. 6(d). We see that only the largest air filling factors $f \equiv f_{\mathrm{B}} \sim 0.67$ can restore a large enough photonic figure of merit in our case, notably because of the broad guide width of 700 nm. The composites with less air have poor F_{phot}. Therefore the overall result of optimization shows that the 1D-composite design approach misses by a large amount the best strategy, with its first wider air slot, and ideally, a thin section of ''silicon-rich'' composite before a wider section of ''bulk'' silicon.

To put it in a complementary perspective, a full optimization would require not only thin slices but more importantly, it would require including technological limits in the figure of merit, with a high price for thin slots for instance. The typical results shown in Fig. 6 suggest that our approach cuts mid-way between such sophisticated options on one hand and the simplicity of the simpler periodic 1D cladding, which is intuitively sub-optimal, on the other hand.

4. Discussion and conclusion

We studied 1D and 2D geometry for the nanostructured cladding of active InP/silicon structures, with the scope of attaining a compromise between thermal sinking and good optical confinement. The possibility to bury nanostructures with the high air/silicon contrast is novel in this kind of devices, and especially attractive in the case of heteroepitaxial InP/Si bonding, without any intermediate layer. Considering first 1D composite claddings made of air slots, we have shown that better confinement would result with slots parallel to the waveguide, but that the demand in terms of slots aspect ratio could be quite high, because air filling factor f in the range 0.1–0.2 should be targeted, while the period should not exceed 200 nm or so, and the heights are of the order of 300 nm. Therefore, we have switched to the case of 2D nanostructured cladding, assuming a square lattice or air cylinders. The two-dimensional aspect greatly relaxes the small feature size issue. For this reason, we investigated the possibility of achieved good confinement based on a reasonably broad central silicon ridge but with deeper etching, 380 nm instead of 280 nm, and with a period of about 200 nm, again suited to avoid any DFB effect.

In the last section, we have presented a more ambitious approach to get our compromise, using the flip-flop algorithm familiar in the area of optical multilayer coatings to define the air/silicon slices sequence in the cladding, and starting from a relatively broad silicon guide ridge width of 700 nm. A model thermal function was used instead of full thermal modelling as we focus here on the optical strategy mostly. The results indicate that improvements over composite 1D structures can be obtained with a first broad air groove adjacent to the ridge, followed by a short gradual transition towards a full silicon cladding outer part. Such a result would need a highly multi-parametric study otherwise.

Further work shall deal with more specific structures (lasers or amplifiers) and fill the missing pieces towards a device, including for instance thermal modelling, a finer account of the technology difficulties regarding thin grooves or small holes, and refined figures of merit for the optical side as well, regarding absorption and also possible thermo-optic effects.

Acknowledgments

This work has been funded by the French ANR-P2N programme within the COHEDIO project. The authors acknowledge useful discussions with G.-H. Duan and A. Lupu.

References

[1] A.W. Fang, H. Park, R. Jones, O. Cohen, M.J. Paniccia, J.E. Bowers, A continuous-wave hybrid AlGaInAs–silicon evanescent laser, IEEE Photonics Technology Letters 18 (2006) 1143–1145.

[2] D. Liang, G. Roelkens, R. Baets, J.E. Bowers, Hybrid integrated platforms for silicon photonics, Materials 3 (2010) 1782–1802.

[3] H. Park, A.W. Fang, S. Kodama, J.E. Bowers, Hybrid silicon evanescent laser fabricated with a silicon waveguide and III–V offset quantum wells, Optics Express 13 (2005) 9460–9464.

[4] A.W. Fang, H. Park, O. Cohen, R. Jones, M.J. Paniccia, J.E. Bowers, Electrically pumped hybrid AlGaInAs–silicon evanescent laser, Optics Express 14 (2006) 9203–9210.

[5] H. Park, A.W. Fang, R. Jones, O. Cohen, O. Raday, M.N. Sysak, M.J. Paniccia, J.E. Bowers, A hybrid AlGaInAs–silicon evanescent waveguide photodetector, Optics Express 15 (2007) 6044–6052.

[6] Y.-H. Kuo, H.-W. Chen, J.E. Bowers, High speed hybrid silicon evanescent electro absorption modulator, Optics Express 16 (2008) 9936–9941.

[7] X. Sun, A. Zadok, M.J. Shearn, K.A. Diest, A.G. Haffari, H.A. Atwater, A. Scherer, A. Yariv, Electrically pumped hybrid evanescent Si/InGaAsP lasers, Optics Letters 34 (2009) 1345–1347.

[8] S. Stankovic, G. Roelkens, D. Van Thourhout, R. Jones, M. Sysak, J. Heck, 1310 nm evanescent hybrid III–V/Si laser based on DVS-BCB bonding, in: Integrated Photonics Research, Silicon and Nano-Photonics (IPR), IWC3, Canada, Toronto, June, 2011.

[9] S. Stankovic, G. Roelkens, D. Van Thourhout, R. Baets, R. Jones, M. Sysak, B. Koch, Hybrid III–V/Silicon laser based on DVS-BCB bonding, in: Proceedings of 13th Annual Symposium of the IEEE/LEOS Benelux Chapter, Enschede, Netherlands, (2008), pp. 139–142.

[10] T. Ilovitsh, I. Bakis, M. Shubely, E. Shekel, Y. Ben-Ezra, C.N. Sukenik, A. Zadok, Wafer bonding techniques for hybrid silicon photonic devices based on surface modifications, in: 14th International Conference on Transparent Optical Networks (ICTON), s, 2–5 July, 2012.

[11] A. Talneau, D. Chouteau, O. Mauguin, L. Largeau, I. Sagnes, G. Patriarche, Heteroepitaxial bonding of GaInAs quantum wells on Si: a new approach towards photonic integration on Si for devices operating at 1.55 μm, Presented at the 24th International Conference on Indium Phosphide and Related Materials, Paper Tu-2E.2, Santa Barbara, CA, USA, August 27–30, 2012.

[12] P. Lalanne, Effective medium theory applied to photonic crystals composed of cubic or square cylinders, Applied Optics 27 (1996) 5369–5380.

[13] D. Bergman, The dielectric constant of a composite material – a problem in classical physics, Physics Reports 43 (1978) 377–407.

[14] W.H. Southwell, Interference filter design using flip-flop optimization, US, Patent, Patent Number 4666250 (1987).

[15] W.H. Southwell, Coating design using very thin high- and low-index layers, Applied Optics 24 (1985) 457–460.

[16] M. Lamponi, S. Keyvaninia, C. Jany, F. Poingt, F. Lelarge, G. de Valicourt, G. Roelkens, D. Van Thourhout, S. Messaoudene, J.-M. Fedeli, G.-H. Duan, Low threshold heterogeneously integrated InP/SOI lasers with a double adiabatic taper coupler, IEEE Photonics Technology Letters 24 (2012) 76–78.

[17] A. David, H. Benisty, C. Weisbuch, Fast factorization rule and plane-wave expansion method for two-dimensional photonic crystals with arbitrary hole-shape, Physical Review B 73 (2006) 075107.

[18] M. Plihal, A.A. Maradudin, Photonic band structure of two-dimensional systems: the triangular lattice, Physical Review B 44 (1991) 8565.